High-resolution x-ray spectroscopy of a subpicosecond-laser-produced silicon plasma

A. Ya. Faenov and I. Yu. Skobelev
Multichanged Ion Spectra Data Center of NPO "VNIIFTRI," Mendeleevo, Moscow Region, 141570, Russia

S. A. Pikuz
P. N. Lebedev Physical Institute of the Russian Academia of Science, Leninskii prospekt 53, Moscow, Russia

G. A. Kyrala, R. D. Fulton, J. Abdallah, Jr., and D. P. Kilcrease
Los Alamos National Laboratory, Los Alamos, New Mexico 87545
(Received 27 October 1994)

The Los Alamos Bright Source laser was used to create a silicon plasma by irradiation of a solid target. A very-high-resolution curved crystal spectrograph was used to detect the emitted x rays. The satellite lines due to the decay of doubly excited states that accompany the Lyman-α lines were observed. The $2p3l$-$1s3l$ radiative transitions in He-like Si were identified. In addition, all the components of the $2l2p\ ^3P-1s2l\ ^3L$ transitions were resolved. The spectra were compared to various collisional-radiative calculations with good results.

PACS number(s): 32.30.Rj, 52.40.Nk

Plasmas created by ultrahigh-intensity subpicosecond laser pulses are very convenient sources for the investigation of radiative transitions from the autoionizing levels of multicharged ions [1–4]. In these dense plasmas satellite lines are produced by the radiative decay of the autoionizing levels into a $1s$ vacancy. Autoionizing levels are generally populated by inner shell excitation, inner shell ionization, and dielectric capture. Since satellite lines are generally excited-to-excited transitions, they are optically thin, and in principle should provide excellent diagnostics of density and temperature, because the radiation is unperturbed by the surrounding plasma. However, these lines are weak compared to resonance lines, and they have very complicated structures. Spectrographs of very high resolution are required to separate structures into component lines, and very accurate calculations are necessary to identify individual lines.

The interaction of laser pulses with solid targets [5–7] produces high-temperature plasmas, having high values of the electron density (up to solid density) and containing highly stripped ions. Some of the transitions due to the initial doubly excited ionic states are relatively intense. These states which have small autoionization rates are populated in the plasma not predominantly by dielectronic capture, but by several other populating mechanisms: (1) collisional mixing with strongly autoionizing levels and (2) direct excitation of ion inner shells by electron impact. The first process is effective only in a dense plasma, the second in an underionized plasma. In the case of subpicosecond-laser-produced plasmas both processes mentioned are effective. This results in doubly excited levels that have large populations, and consequently, the satellite spectral lines, caused by radiative decay of these levels, have relatively high brightness.

The subpicosecond-laser-produced plasmas are, of course, very bright x-ray emitters, but since the pulse length is short the total energy of emitted photons can be small. Therefore it is necessary to have a sensitive spectrograph to observe spectral lines from doubly excited levels. Additionally, this spectrograph must have very good spectral resolution $\lambda/\Delta\lambda \geq 5000$, because the large number of satellite lines are concentrated in a very narrow spectral region near the appropriate resonance line. Such spectrographs, called FSSR-1D, were constructed in the past few years at the Multicharged Ion Spectra Data Center (MISDC) [8]. Spherically bent mica crystals are used to disperse and to focus with a spectral resolution of up to $\lambda/\Delta\lambda \approx 10\,000-20\,000$.

Using an FSSR-1D spectrograph to observe subpicosecond-laser-produced plasma allowed us for the first time to observe and identify the resolved satellite lines caused by the $2p3l$-$1s3l$ radiative transitions in He-like Si XIII ions and also to resolve all components of the $2p2l\ ^3P-1s2l\ ^3L$ transitions. Comparison of the intensities of observed spectral lines with time-independent calculations showed that the emission of these lines mostly occurs at plasma electron density $N_e \approx 6\times10^{22}$ cm^{-3} and plasma electron temperature $T_e \approx 460$ eV.

The experiment was performed at the Los Alamos Bright Source II facility. The eximer XeCl laser system was used to create a high-temperature plasma. A frequency-doubled seed pulse generated with a synchronously pumped dye laser oscillator-amplifier combination is amplified with transversely pumped XeCl amplifiers. The detailed performance of the laser is described in Ref. [9]. The laser operates at a wavelength of 308 nm, and produces a 300-fs pulse containing 0.25 J, at a repetition rate of 1 Hz. When focused on a silicon target, with $f/1.9$ optics, it generates irradiances exceeding 4×10^{18} W/cm^2. The amplified stimulated emission (ASE) from the amplifier generates a prepulse plasma in front of the target with which the main pulse interacts.

The plasma emission spectra in the x-ray region were measured by the focusing spectrograph with spatial reso-

lution (FSSR-1D). See Refs. [8,10–12] and Fig. 1 for more details about this scheme. The crystal, film, and source must be placed at special positions [see Fig. 1(a)]. A definite relation between the glancing angle θ and the distance from the source to the top of the sphere A must be satisfied for each wavelength:

$$A = -R \sin(\theta)/\cos 2\theta \ .$$

The glancing angle θ is related to the incident wavelength by Bragg's law $2d \sin\theta = n\lambda$, where $2d$ is twice the interplanar distance for the crystal, n is the order of reflection, and R is the radius of curvature of crystal. In the present case, a spherical mica crystal with dimensions of 10×30 mm and a radius of curvature of 100 mm was used. The spectra near the resonance line of the H-like ion (Si XIV) were measured in the third order of reflection of the mica crystal. The Bragg angle was about 69° and the spectral dispersion on the film was 0.024 Å/mm. The high quality of the spherical mica crystal used produced a spatial resolution [10,11] better than 18 μm and a spectral resolution [13] given by $\lambda/\Delta\lambda$ of up to 10 000. The spectrograph was very sensitive and the plasma emission was so intense that the spectra could be recorded in a single laser shot.

An example of the plasma emission spectrum in the region $\lambda = 6.16$–6.27 Å near the Ly-α line of the H-like Si XIV ion is shown in Fig. 2(b). For comparison in this

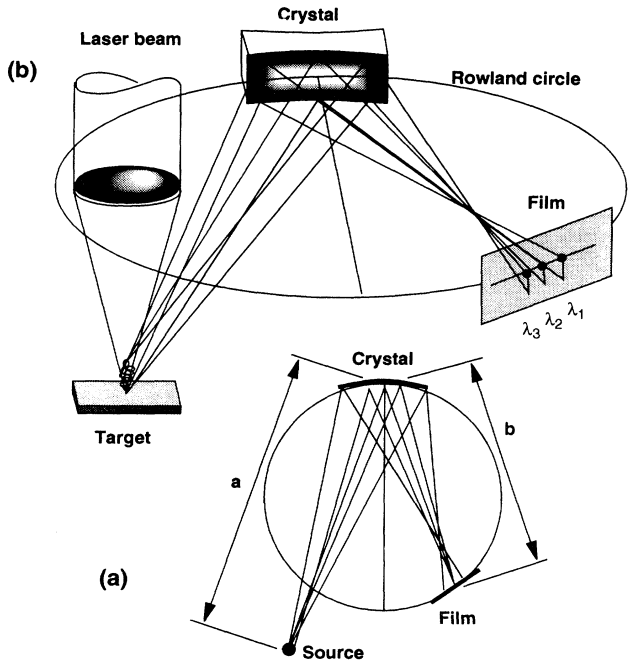

FIG. 1. (a) Schematic of the focusing spectrograph with spatial resolution (FSSR-1D), (b) example of using FSSR-1D as a diagnostic for a laser-produced plasma.

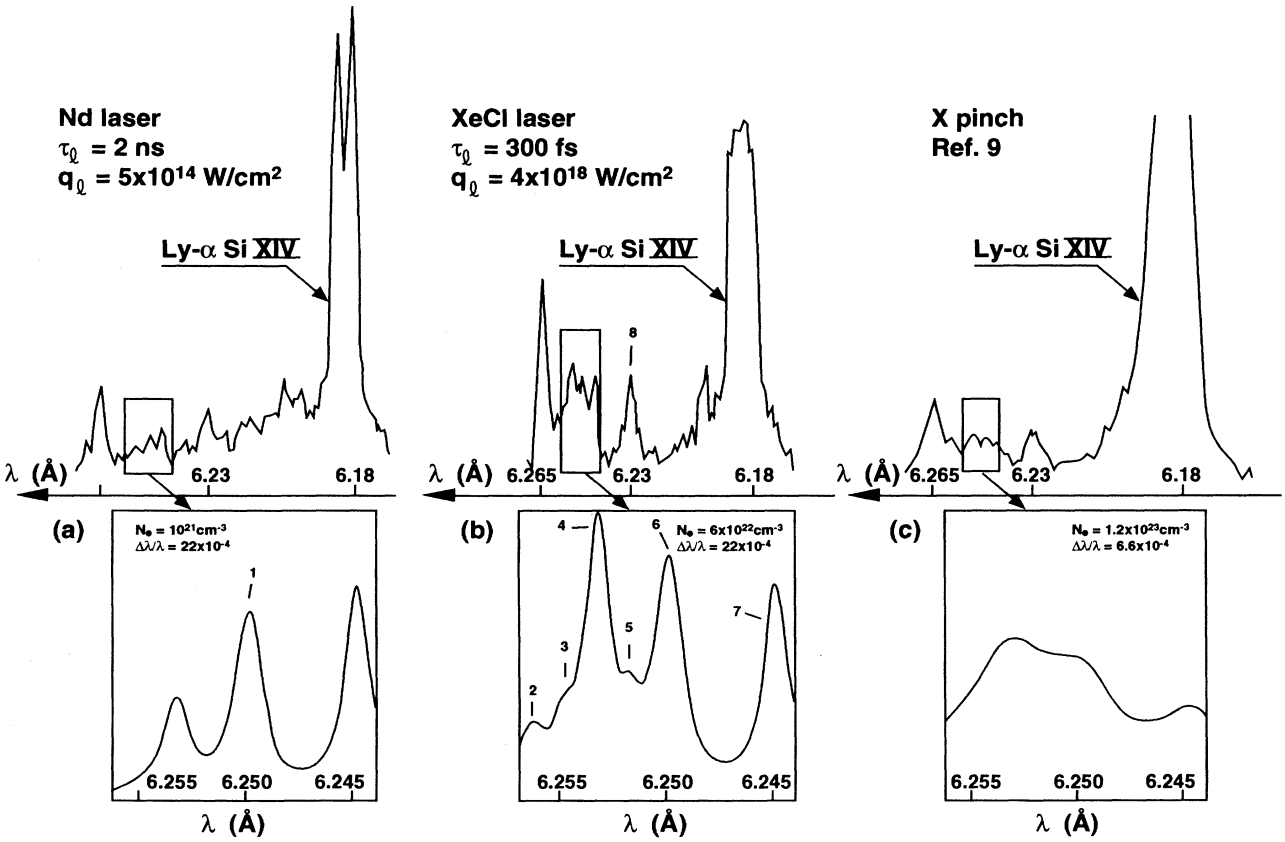

FIG. 2. Silicon plasma emission spectrum in the region $\lambda = 6.16$–6.27 Å observed in different plasma sources: (a) Nd-laser-produced plasma (obtained in Ref. [8] for five shots), (b) XeCl-laser-produced plasma (obtained in present work for two shots), (c) X-pinch plasma (obtained in Ref. [9] in one shot) and (below) the results of theoretical calculations for $2l2p\ ^3P - 1s2l\ ^3L$ lines.

figure we also present analogous spectra observed earlier in a plasma heated by a 2-ns pulse from a Nd laser [12] [Fig. 2(a)] and in an X-pinch plasma [14,15] [Fig. 2(c)]. We see that the spectrum in Fig. 2(b) contains a number of resolved spectral lines having significant intensities. Some of the lines (lines 1–8) are the satellites caused by $2p2l$-$1s2l$ transitions in the Si XIII ion (for the spectroscopic notation for these lines see below in Table I). It should be noted that only lines 1, 4, and 6–8 were identified earlier in Nd-laser-produced plasma, because it is necessary to have a dense plasma with $N_e \gg 10^{21}$ cm^{-3} to observe the weakest components of the triplets $2l2p\ ^3P-1s2l\ ^3L$ (lines, 2, 3, and 5). It will be shown below that other lines contained in the spectrum in Fig. 2(b) are caused by $2p3l$-$1s3l$ transitions in Si XIII.

The most intense lines $2p^2\ ^1D_2-1s2p\ ^1P_1$ and $2s2p\ ^1P_1-1s2s\ ^1S_0$ (lines 1 and 8) were used as reference lines to measure the wavelengths of others. For these lines we used the calculated wavelength values [16] which were shifted by 0.0005 Å according to the more precise treatment [17] for the energy of the $1s2p\ ^1P_1$ level. In this case, the observed spectral range is very small and the divergency of our spectrograph dispersion curve from the Johann type is small enough that the relative accuracy of wavelength measurements is about 0.0008 Å. The absolute accuracy is not know exactly due to uncertainty of reference lines, but we believe that it is better than 0.0015 Å.

X-ray spectroscopic methods are used in the present paper to estimate laser-produced plasma parameters. Since we observed plasma emission spectra without time and spatial resolution only average values of the plasma parameters can be obtained. To determine the electron plasma temperature we used the integrated line intensity ratio of the satellite $2p^2\ ^1D_2-1s2p\ ^1P_1$ to the resonance Ly-α line (see, for example, Ref. [12]). Comparing the experimental value of this intensity ratio with theoretical ones we found $T_e=460$ eV. The actual value of the temperature may be somewhat higher than this value due to the optical depth and possible saturation of the Ly-α line.

For a diagnostic of the electron plasma density we used the density-sensitive dielectronic satellites $2p^2\ ^3P-1s2p\ ^3P$ and $2s2p\ ^3P-1s2s\ ^3S$. At first, we compared the experimental values of the intensity ratio

TABLE I. Dielectronic satellites caused by radiative transitions in He-like ion Si XIII. The numbers in parentheses are LANL calculations.

	Wavelengths			
N_e	Expt. (Å)	Theor., Refs. [16,20] (Å)	⟨Expt.-theor.⟩ (mÅ)	Transitions
1	6.2654[a]	6.2654[b](6.2626)		$2p^2\ ^1D_2-1s2p\ ^1P_1$
2	6.2564	6.2560(6.2552)	0.4	$2p^2\ ^3P_1-1s2p\ ^3P_2$
3	6.2549	6.2550(6.2541)	−0.1	$2p^2\ ^3P_0-1s2p\ ^3P_1$
4	6.2532	6.2532(6.2523)	0.1	$2p^2\ ^3P_1-1s2p\ ^3P_1$
		6.2530(6.2521)		$2p^2\ ^3P_2-1s2p\ ^3P_2$
5	6.2517	6.2525(6.2510)	−0.8	$2p^2\ ^3P_1-1s2p\ ^3P_0$
6	6.2501	6.2502(6.2491)	0.8	$2p^2\ ^3P_2-1s2p\ ^3P_1$
		6.2497(6.2490)		$2s2p\ ^3P_0-1s2s\ ^3S_1$
		6.2481(6.2474)		$2s2p\ ^3P_1-1s2s\ ^3S_1$
7	6.2447	6.2446(6.2438)	0.1	$2s2p\ ^3P_2-1s2s\ ^3S_1$
8	6.2296[a]	6.2296(6.2278)		$2s2p\ ^1P_1-1s2s\ ^1S_0$
9	6.2221	6.2238(6.2231)	−1.7	$2s3p\ ^1P_1-1s3s\ ^1S_0$
10	6.2186	6.2165(6.2166)	2.1	$2p3p\ ^1P_1-1s3p\ ^1P_1$
11	6.2117	6.2119(6.2118)	−0.2	$2p3p\ ^3D_1-1s3p\ ^3P_0$
12	6.2095	6.2097(6.2096)	−0.2	$2p3p\ ^3D_2-1s3p\ ^3P_1$
13	6.2080	6.2078(6.2076)	0.2	$2p3p\ ^3D_3-1s3p\ ^3P_2$
14	6.2039	6.2042(6.2034)	−0.4	$2p3d\ ^3F_2-1s3d\ ^3D_1$
		6.2043(6.2035)		$2p3d\ ^3F_2-1s3d\ ^3D_2$
15	6.2003	6.2019(6.2009)	−0.5	$2p3d\ ^3F_3-1s3d\ ^3D_2$
		6.2015(6.2012)		$2p3p\ ^1D_2-1s3p\ ^1P_1$
		6.1991[b](6.1992)		$2p^2\ ^1S_0-1s2p\ ^1P_1$
16	6.1986	6.1993(6.1999)	−0.6	$2p3d\ ^1D_2-1s3d\ ^1D_2$
		6.1992(6.1982)		$2p3d\ ^3F_4-1s3d\ ^3D_3$
17	6.1963	6.1974(6.1976)	−0.6	$2s3p\ ^3P_2-1s3s\ ^3S_1$
		6.1963(6.1972)		$2s3p\ ^3P_0-1s3s\ ^3S_1$
18	6.1948	6.1952(6.1961)	−0.4	$2p3s\ ^3P_1-1s3s\ ^3S_1$
19	6.1928	6.1928(6.1928)	0.0	$2p3p\ ^1D_2-1s3p\ ^3P_2$
		6.1928(6.1935)		$2p3s\ ^3P_2-1s3s\ ^3S_1$
20	6.1677	6.1676(6.1676)	0.1	$2p3d\ ^1P_1-1s3d\ ^1D_2$
21	6.1650	6.1644(6.1640)	0.6	$2p3p\ ^1S_0-1s3p\ ^1P_1$

[a]Reference lines.
[b]Shifted by 0.005 Å according to calculation in Ref. [17] for the energy of $1s2p\ ^1P_1$ level.

$I(2p^2\,{}^3P_{0,1,2} \rightarrow 1s2p\,{}^3P_{0,1,2})/I(2s2p\,{}^3P_{0,1,2} \rightarrow 1s2s\,{}^3S_1)$ with calculations of Ref. [18] and found $N_e = 6\times10^{22}$ cm^{-3}. After that we used the results of Ref. [18] and this N_e value to calculate the intensities of all components of these triplets separately and to simulate plasma emission spectra in the region $\lambda = 6.24$–6.26 Å. Analogous procedures were also carried out for the cases of the Nd-laser-produced plasma and X-pinch plasma. Results obtained are shown in Fig. 2. In all cases the correspondence between theoretical and experimental data is very good. It confirms the reliability of (1) this diagnostic method and (2) the value $N_e = 6\times10^{22}$ cm^{-3} obtained for the case of our subpicosecond laser experiment. It should be noted also that the experimental Stark width of the Si XIV Ly-α line is consistent with the calculated Stark width due to electron and quasistatic ions [19] at $N_e = 6\times10^{22}$ cm^{-3}. Note that plasma parameters could also be derived from a similar analysis involving the He$_\alpha$ satellite lines.

As can be seen from Fig. 2(b), the observed plasma emission spectrum contains some lines in the spectral region 6.16–6.23 Å (these lines are marked by numbers 9–21 in Fig. 3). The results of wavelength calculations from Ref. [20] allow us to suppose that these lines (all or some of them) are caused by the radiative decay of $2l3l'$ levels of the Si XIII ion. Actually, the comparison of their experimental wavelength values with theoretical ones shows that all observed lines correspond to some $2l3l'$-$1s3l'$ transitions. However, the comparison of their intensities with line intensities in the coronal limit shows that the theoretical values strongly differ from the experimental ones [see Fig. 3(b) which shows the plasma emission spectra calculated with the help of a coronal kinetic model]. This disagreement is expected because a coronal model is not applicable in the case of a high-density plasma with $N_e = 6\times10^{22}$ cm^{-3}. In reality, for such dense plasma, collisional mixing of double excited ion states is even more effective than noncollisional decay, and a general radiative-collision kinetic model must be used to calculate the level populations and, consequently, spectral lines intensities. Such calculations were carried out in the present paper and the results obtained for plasma with $N_e = 6\times10^{22}$ cm^{-3}, $T_e = 460$ eV and for Lorentz line shapes are shown in Fig. 3. Now we see that the correspondence of theoretical line intensities with experimental data is excellent. It allows us to identify lines 9–21 as satellites caused by $2l3l'$-$1s3l'$ transitions in the He-like ion Si XIII. The results of our identification and wavelength measurements are presented in Table I.

As an independent check, a collisional-radiative model was constructed using Los Alamos atomic physics codes which are based on the semirelativistic Hartree-Fock method of Cowan [21]. The model included configurations of the type $1s^2$, $1s2l$, $1s3l$, $2l2l'$, $2l3l'$, and $3l3l'$ for the He-like ion stage. The values of l and l' range over all possibilities for the given values of principle quantum number. The model also includes all configurations through $3d$ for the H-like ion stage. The corresponding detailed fine-structure levels including intermediate coupling, spin-orbit coupling, and configuration interaction were used in the modeling cal-

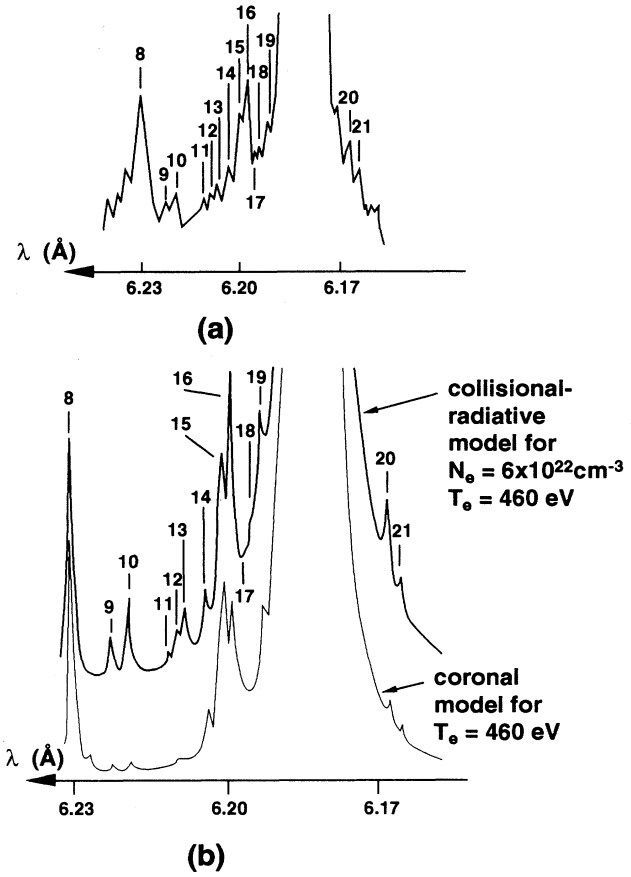

FIG. 3. (a) Silicon subpicosecond-laser-produced plasma emission in the region 6.16–6.23 Å, (b) plasma emission spectra calculated by both coronal and collisional-radiative kinetic models.

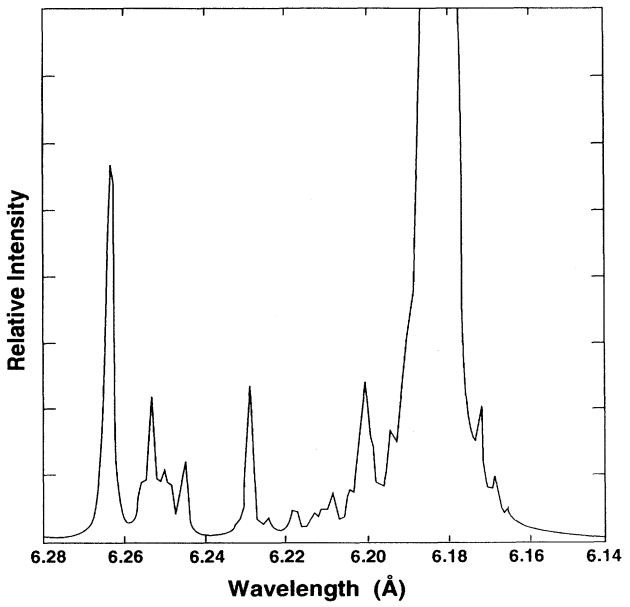

FIG. 4. The plasma emission spectra calculated using a Los Alamos based collision-radiative model.

culations. Oscillator strengths were calculated for all dipole-allowed transitions. Distorted-wave collision strengths were calculated for all transitions starting in the $1s^2$, $1s2s$, and $1s2p$ levels to all upper levels. Plane-wave-Born collision strengths were used for all other transitions. Collisional ionization and photoionization cross sections were calculated for transitions between the appropriate levels in the adjacent ion stages. Auger rates were calculated for all autoionizing levels in the He-like ion.

The steady state model included collision excitation, deexcitation, spontaneous radiative decay, autoionization, dielectronic recombination, collisional ionization, three-body recombination, and radiative recombination. The models are discussed in greater detail in Ref. [22]. The atomic data discussed above were used to calculate rate coefficients and solve the kinetics equations at $T_e = 460$ eV and $N_e = 6 \times 10^{22}$ cm^{-3}. The resultant populations were used to compute the spectra shown in Fig. 4. The results correlate well with this experiment shown in Fig. 2 and the Russian collisional-radiative model shown in Fig. 3. The calculations also show that all satellite lines are optically thin assuming a 10-μm plasma size for the present experimental conditions.

In conclusion, the use of a subpicosecond-laser-produced plasma and the high-resolution, high-luminosity FSSR-1D spectrograph allowed us for the first time to observe and identify the satellites to the Ly-α Si XIV resonance line, caused by $2p3l$-$1s3l$ radiative transitions, and to measure their wavelengths with a relative accuracy of ± 0.0008 Å and an absolute accuracy of ± 0.0015 Å. For improvement of the absolute measurement accuracy we need to exclude the uncertainties in the wavelengths of the reference lines. This can be done in the future both experimentally and by using modern quantum electrodynamic *ab initio* methods for wavelength calculations of the reference lines $2p^2\,{}^1D_2 - 1s2p\,{}^1P_1$ and $2s2p\,{}^1P_1 - 1s2s\,{}^1S_0$.

In addition, we have found the average plasma temperature and density to be approximately 460 eV and 6×10^{22} cm^{-3}, respectively, for the case of a plasma formed by the 400-fs pulse of a XeCl laser with a flux density $q_e \simeq 4 \times 10^{18}$ W/cm^2. The small value of electron temperature and the large value of electron density (greater than critical density for $\lambda_l = 308$ nm) indicate that in our experiments the x-ray plasma emission occurs mostly in the spatial region between the critical point and the solid surface.

This work was supported in part by the U.S. Department of Energy.

[1] F. Bely-Dubau, A. H. Gabriel, and S. Volonte, Mon. Not. R. Astron. Soc. **189**, 801 (1979).

[2] M. Bitter, F. Beli-Dubau, S. Cohen, K. W. Hill, M. Lovlergue, U. I. Safronova, S. Sesnic, L. Steenmanclark, F. Tenney, J. Timberlake, L. A. Vainshtein, and S. Von Goeler, Phys. Rev. A **29**, 661 (1984).

[3] B. A. Bryunetkin, I. Yu. Skobelev, A. Ya. Faenov, M. P. Kalashnikov, P. Nickles, M. Schnuerer, and S. A. Pikuz, Sov. J. Quantum Electron. **23**, 337 (1993).

[4] J. Abdallah, Jr., B. A. Bryunetkin, M. P. Kalashnikov, R. Clark, P. Nickles, S. A. Pikuz, I. Yu. Skobelev, A. Ya Faenov, and M. Schnuerer, Sov. J. Quantum Electron **20**, 1150 (1993).

[5] G. A. Kyrala, R. D. Fulton, E. K. Wahlin, L. A. Jones, G. T. Schappert, J. A. Cobble, and A. J. Taylor, Appl. Phys. Lett. **60**, 2195 (1992).

[6] A. Zigler, P. G. Burkhalter, D. J. Nagel, M. D. Rosen, K. Boyer, T. S. Luk, A. McPherson, and C. K. Rhodes, Opt. Lett. **16**, 1261 (1991).

[7] M. Chaker, J. C. Kieffer, J. P. Matte, H. Pepin, P. Audebert, P. Maine, D. Strickland, P. Bado, and G. Mourou, Phys. Fluids B **3**, 167 (1990).

[8] B. A. Bryunetkin, A. Ya. Faenov, S. A. Pikuz, and I. Yu. Skobelev, Laser Part. Beams **10**, 849 (1992).

[9] A. J. Taylor, C. R. Tallman, J. P. Roberts, C. S. Lester, T. R. Cosnell, P. H. Y. Lee, and G. A. Kyrala, Opt. Lett. **15**, 39 (1990).

[10] A. Ya. Faenov, S. A. Pikuz, A. I. Erko, B. A. Bryunetkin, V. M. Dyakin, G. V. Ivanenkov, A. R. Mingaleev, T. A. Pikuz, V. M. Romanova, and T. A. Shelkovenko, Phys. Scr. **50**, 106 (1994).

[11] T. A. Pikuz, A. Ya. Faenov, S. A. Pikuz, V. M. Romanova, and T. A. Shelkovenko (unpublished).

[12] V. A. Boiko, A. V. Vinogradov, S. A. Pikuz, I. Yu. Skobelev, and A. Ya. Faenov, J. Sov. Laser Res. **23**, 201 (1993).

[13] B. A. Bryunetkin, A. Ya. Faenov, M. Kalashnikov, P. Nickles, M. Schnuerer, I. Yu. Skobelev, J. Abdallah, Jr., and R. E. H. Clark, J. Quant. Spectrosc. Radiat. Transfer **53**, 45 (1995).

[14] S. A. Pikuz, B. A. Bryunetkin, G. V. Ivanenkov, A. R. Mingaleev, V. M. Romanova, I. Yu. Skobelev, A. Ya. Faenov, S. Ya. Khakhalin, and T. A. Shelkovenko, Sov. J. Quantum Electron. **23**, 201 (1993).

[15] S. A. Pikuz, B. A. Bryunetkin, G. V. Ivanenkov, A. R. Mingaleev, V. M. Romanova, I. Yu. Skobelev, Y. A. Faenov, S. Ya. Khakalin, and T. A. Shelkovenkso, J. Quant. Spectrosc. Radiat. Transfer **51**, 291 (1994).

[16] L. A. Vainshtein and U. I. Safronova (unpublished).

[17] V. A. Boiko, V. G. Palchikov, I. Yu. Skobelev, and A. Ya. Faenov, *Spectroscopic Constants of Atoms and Ions,* M. Izd. Standartov, 1988 (in Russian).

[18] A. V. Vinogradov, I. Yu. Skobelev, and E. A. Yukov, Zh. Eksp. Teor. Fiz. **72**, 1762 (1977) [Sov. Phys. JETP **45**, 925 (1977)].

[19] R. C. Mancini, D. P. Kilcrease, L. A. Woltz, and C. F. Hooper, Jr., Comput. Phys. Commun. **63**, 314 (1991).

[20] L. A. Vainshtein and U. I. Safronova (unpublished).

[21] R. D. Cowan, *Theory of Atomic Spectra* (University of California Press, Berkeley, 1981).

[22] J. Abdallah, Jr., R. E. H. Clark, C. J. Keane, T. D. Shepard, and L. J. Suter, J. Quant. Spectrosc. Radiat. Transfer **50**, 91 (1993).